Frequency doubling of femtosecond pulses in walk-off-compensated *N*-(4-nitrophenyl)-*L*-prolinol

Juan P. Torres, Silvia Carrasco, and Lluis Torner

Laboratory of Photonics, Department of Signal Theory and Communications, Universitat Politecnica de Catalunya, Gran Capitan UPC-D3, Barcelona ES 08034, Spain

Eric W. VanStryland

Center for Research and Education in Optics and Lasers, University of Central Florida, Orlando, Florida 32826

Received June 29, 2000

We show how to exploit the high quadratic nonlinear coefficient of the organic crystal *N*-(4-nitrophenyl)-*L*-prolinol for generation and parametric mixing of ultrashort pulses by use of tilted-pulse techniques. The effective crystal length for subpicosecond operation is shown to be enhanced from tens of micrometers to tens of millimeters. Efficient frequency doubling of 100-fs pulses is predicted in walk-off-compensated geometries with peak intensities of a few megawatts per square centimeter. © 2000 Optical Society of America

OCIS codes: 190.2620, 190.7110, 320.2250, 160.4890.

N-(4-nitrophenyl)-*L*-prolinol (NPP) is an organic molecular crystal developed by molecular engineering[1] that exhibits one of the highest phase-matchable second-order susceptibilities reported so far in the near-infrared spectral range ($d_{\mathrm{eff}} \approx 56$ pm/V).[2] Because of such large nonlinearity, NPP holds promise for the implementation of parametric devices for frequency conversion and mixing with pump signals with significantly reduced intensities relative to those needed with conventional quadratic materials. An important step in this direction was reported recently by Banfi *et al.*, who realized a highly efficient frequency shifter in a 2.8-mm-thick NPP crystal.[3] The device operated in a nearly degenerate frequency-mixing configuration in which a frequency-doubled pump light interacted with a synchronous signal to produce a frequency-shifted output. To avoid walk-off effects they performed the experiments with pump and signal wavelengths set near the noncritical phase-matching wavelength of the material ($\lambda_{\mathrm{ncpm}} \approx 1.15$ μm), with pulses having a duration of 20 ps. However, as was pointed out by Wang *et al.*,[4] the large spatial and temporal walk-off that exist in NPP severely limit the usefulness of the material away from the noncritical phase-matching wavelength and for shorter pulses. Such limitations are twofold. First, walk-off causes the fundamental frequency (FF) and the second-harmonic (SH) signals to walk off from each other while propagating inside the crystal, thus reducing the useful nonlinear crystal length in which efficient interaction takes place. Second, the presence of group-velocity mismatch (GVM) can largely distort the shape and duration of the SH pulses generated in crystals that are thicker than the pulse walk-off length. As a consequence, extremely short crystal thicknesses must be employed with subpicosecond pulses.

Here we show that subpicosecond pulses can be efficiently frequency doubled and mixed in NPP with moderate pump intensities. This method benefits from the large Poynting vector walk-off exhibited by NPP crystals outside noncritical phase matching, because it employs tilted-pulse techniques. This technique spectral disperses the pump FF signals in different directions by passing them through a medium with angular dispersion, such as a prism[5] or a properly designed diffraction grating.[6,7] One needs to tailor the amount of angular dispersion to obtain effective GVM compensation. Tilted-pulse techniques have been used extensively in recent years for efficient doubling of ultrashort pulses[8] and the observation of quadratic temporal and spatiotemporal solitons mediated by cascading nonlinearities in β-barium borate (BBO) and $LiIO_3$, respectively.[9,10]

Here we study SH generation pumped by pulsed FF light. In the wavelength band 1–2 μm, type I *ooe* (*eeo*) phase matching in NPP is achieved when light propagates in the *yz* (*xz*) plane. In the proposed scheme the pump light that is input into the crystal is a highly elliptical beam, so diffraction along one of the transverse axes is negligible. The evolution of the envelopes of the FF and the SH signals is described by[11]

$$i\frac{\partial A_1}{\partial z} - \frac{k_1''}{2}\frac{\partial^2 A_1}{\partial t^2} + \frac{1}{2k_1}\frac{\partial^2 A_1}{\partial x^2} + i\frac{\Gamma_1}{2}A_1 + K_1 A_1^{*} A_2 \exp(-i\Delta k z) = 0, \quad (1)$$

$$i\frac{\partial A_2}{\partial z} - \frac{k_2''}{2}\frac{\partial^2 A_2}{\partial t^2} + \frac{1}{2k_2}\frac{\partial^2 A_2}{\partial x^2} - i\rho_t\frac{\partial A_2}{\partial x} - i\rho_x\frac{\partial A^2}{\partial x} + i\frac{\Gamma_2}{2}A_2 + K_2 A_1^{2}\exp(i\Delta k z) = 0, \quad (2)$$

where A_ν, with $\nu = 1, 2$, are the amplitudes of the FF and the SH waves, respectively; z is the longitudinal coordinate; t is the retarded time; x is the spatial transverse coordinate; and Γ_ν are absorption coefficients. The parameters k_ν are the linear wave numbers, k_ν' are the inverse group velocities, k_ν'' are the group-velocity dispersion (GVD's), and $\Delta k = 2k_1 - k_2$ is the wave-vector mismatch. The walk-off parameters are given by $\rho_t = k_1' - k_2'$ and $\rho_x = \tan(\rho_2) - \tan(\rho_1)$, where ρ_1 and ρ_2 are the

0146-9592/00/231735-03$15.00/0

Poynting vector walk-off angles. Finally, $K_\nu = 4\pi d_{\text{eff}}/\lambda n_\nu$, where λ is the FF wavelength, n_ν are the refractive indices and d_{eff} is the second-order susceptibility.

Tilted-pulse techniques are based on diffraction of the input FF wave, $A_1(z;x,t)$, by a grating so that each spectral component is dispersed in a different direction.[6–10] The resulting signal is a tilted pulse, $A_1[z;x,t - x\tan(\psi)/c]$, where ψ is the tilt angle and c is the velocity of light, so that its peak intensity is located at a different time for each value of x. For normal incidence on the nonlinear crystal, one has[6]

$$\tan(\psi) = -m\,\frac{\lambda}{d\cos\beta}\,, \tag{3}$$

where d is the groove spacing of the grating, m is the diffraction order, and β is the diffraction angle. When the beam width in the x direction of the incident signal on the grating is large enough (i.e., a few millimeters), the effect of diffraction can be accounted for by consideration of temporal evolution only but with new effective inverse group velocities and GVD's,

$$u_\nu = k_\nu{}' + \tan(\psi)\tan(\rho_\nu)/c\,, \tag{4}$$

$$g_\nu = k_\nu{}'' - \frac{1}{k_\nu}\,\frac{[\tan(\psi)]^2}{c}\,, \tag{5}$$

respectively. The SH wave is assumed to acquire the same tilt as the FF. Therefore, the spatiotemporal light evolution can be described by

$$i\,\frac{\partial A_1}{\partial z} - \frac{g_1}{2}\,\frac{\partial^2 A_1}{\partial t^2} + i\,\frac{\Gamma_1}{2}\,A_1 + K_1 A_1{}^* A_2\exp(-i\Delta k z) \simeq 0\,, \tag{6}$$

$$i\,\frac{\partial A_2}{\partial z} - \frac{g_2}{2}\,\frac{\partial^2 A_2}{\partial t^2} - i\rho_u\,\frac{\partial A_2}{\partial t} + i\,\frac{\Gamma_2}{2}\,A_2 + K_2 A_1{}^2\exp(i\Delta k z) \simeq 0\,, \tag{7}$$

with $\rho_u = u_1 - u_2$. Notice that the contribution of the tilt angle to the effective GVD is always negative.

To elucidate whether input light and material conditions suitable for efficient SH generation exist, we proceed as follows: First, we calculate the phase-matching angle θ_{pm} at the pump wavelength, using the Sellmeier equations for NPP as measured by Datta *et al.*[12] Second, we find the value of the tilt, ψ_0, required for GVM cancellation ($u_1 = u_2$). This gives the effective GVD's, g_ν. Figure 1 shows the outcome for $\tau = 100$ fs pulses (τ is the FWHM duration of the signal intensity). Figure 1(a) shows the tilt ψ_0 required as a function of pump wavelength in the band $\lambda = 1$–2 μm, and Fig. 1(b) shows the corresponding effective dispersion lengths, $L_{\text{d}\nu} = 0.161\tau^2/g_\nu$, experienced by the FF and the SH signals. The effective GVD at the FF is found to be anomalous ($g_1 < 0$) over the whole wavelength band that is displayed, whereas the effective GVD at the SH frequency turns out to be anomalous inside the band $\lambda \approx 1.07$–1.23 μm and normal otherwise. At λ_{ncpm} the Poynting vector walk-off vanishes, hence GVM cancellation is not possible. Thus, both the tilt, ψ_0, and the GVD's, g_ν, are undefined. It is worth noticing the narrow wavelength band around λ_{ncpm}, where both the FF and the SH signals experience very high effective anomalous dispersion. Such huge dispersion may allow, for the first time, the observation of quadratic solitons over many dispersion lengths, provided that the corresponding diffraction gratings can be made.

The important conclusion revealed by Fig. 1 is that suitable conditions for efficient SH generation, namely, negligible GVM and dispersion lengths of several millimeters, exist in a wide pump wavelength band centered at the third telecommunication window. Importantly, the required tilt ψ_0 is shown to be a smooth function of the pump wavelength. This smooth function is an indication of the robustness of the proposed scheme. Such robustness is confirmed by Fig. 2(a), which shows the variation of the dispersion lengths and of the walk-off length, defined as $L_w = 0.567\tau/(u_1 - u_2)$, versus deviations of the nominal tilt required for exact walk-off cancellation at a given wavelength. In Fig. 2(a), $\lambda = 1.6$ μm, but similar results are obtained for other wavelengths inside the band. Notice that tilt acceptance of several degrees is obtained with walk-off lengths in excess of 5 mm. Similarly, Fig. 2(b) shows that for a fixed tilt a wavelength bandwidth of several tens of nanometers is obtained. Naturally, all tolerances increase when either the acceptable walk-off length is reduced or the pulse width is increased.

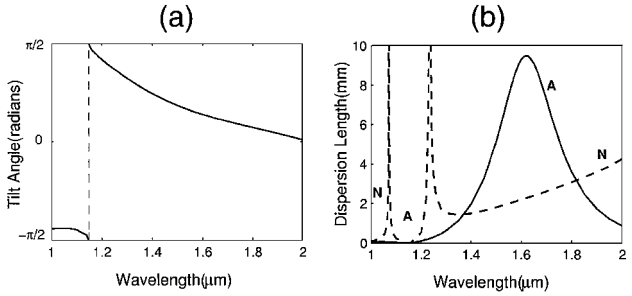

Fig. 1. (a) Tilt angle required for exact GVM cancellation in phase-matched type I SH generation in NPP as a function of pump wavelength. (b) Corresponding effective dispersion lengths at the FF and the SH. Solid curves, FF; dashed curves, SH. Pulse duration $\tau = 100$ fs. A and N stand for anomalous and normal dispersion, respectively.

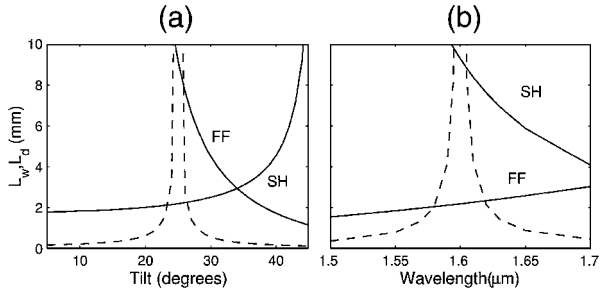

Fig. 2. (a) Effective dispersion lengths at the FF and the SH and (dashed curves) temporal walk-off length as a function of tilt angle for a fixed pump wavelength, $\lambda = 1.6$ μm. (b) Dispersion and walk-off lengths as a function of pump wavelength for a fixed tilt angle $\psi_0 = 24.9°$. In both cases, $\theta = \theta_{\text{pm}}$ and $\tau = 100$ fs.

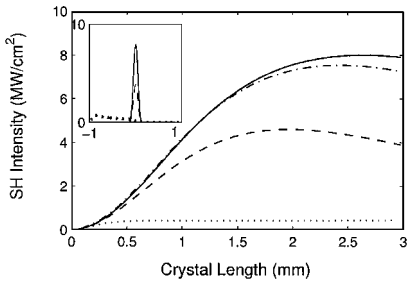

Fig. 3. Simulated evolution of the peak intensity of the FF and the SH signals as a function of crystal length. Solid curves, (1 + 1) temporal evolution with GVM compensation; dotted–dashed curves, (2 + 1) spatiotemporal full evolution with GVM compensation; dotted curves, evolution without GVM compensation; dashed curves, (1 + 1) temporal evolution with GVM compensation including absorption. Inset, output SH pulses. Conditions: phase matching, $I_0 = 10$ MW/cm^2, $w_0 = 3$ mm, and $\tau = 100$ fs.

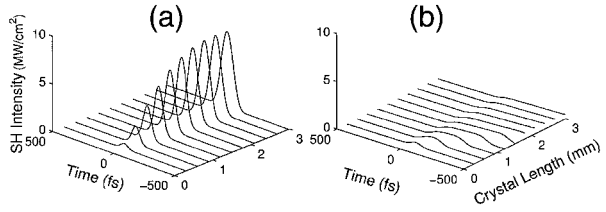

Fig. 4. Detailed evolution of the SH pulse under the conditions of Fig. 3 (a) with and (b) without GVM compensation.

To show that efficient SH generation occurs under the conditions suggested by Figs. 1 and 2, we solved expressions (6) and (7) numerically with a split-step Fourier method. The input conditions contain only FF light with the shape $A_1(z = 0, t) = {I_0}^{1/2}\,\mathrm{sech}(t/\tau_0)$, where I_0 is the input peak intensity and $\tau_0 = \tau/1.763$. The derivation of expressions (6) and (7) from Eqs. (1) and (2) assumes a plane wave that is incident on the diffraction grating. Actually, in practice the input beam is a Gaussian beam. To verify the accuracy of expressions (6) and (7) we also solved the full system of equations (1) and (2) for input conditions corresponding to light distribution produced by the diffraction grating, namely, $A_1(z = 0, x, t) = {I_0}^{1/2}\,\mathrm{sech}\{[t - x\,\tan(\psi)/c]/\tau_0\}\exp(-x^2/{w_0}^2)$, where w_0 is the waist of the Gaussian beam that is incident on the grating. Because of the departures of the Gaussian shape from a plane wave, the characteristics length at which the system of expressions (6) and (7) fails is $L \sim w_0/\tan(\rho)$. Otherwise, perfect agreement between the predictions of expressions (6) and (7) and those of Eqs. (1) and (2) was always obtained.

Figure 3 shows the typical outcome of the simulations. The figure shows phase-matched upconversion of a $\lambda = 1.6$ μm pump with peak intensity $I_0 = 10$ MW/cm^2 in a 3-mm-long NPP crystal. The pulse width is set to $\tau = 100$ fs in a beam with width $w_0 = 3$ mm. In the simulations we took into account the absorption of NPP owing to its molecular structure be letting $\Gamma_1 = 1.5$ cm^{-1} and $\Gamma_2 = 3.0$ cm^{-1}. The dotted curves correspond to the SH that was generated without GVM compensation. Figure 4 shows the detailed SH pulse evolution with and without GVM compensations. A drastic difference is clearly visible: Although no useful SH is generated without walk-off compensation, a clean, narrow high-intensity SH pulse is obtained with the tilted pulse. Losses would reduce the efficiency of SH generation in thick crystals, but a high-quality output SH pulse would always be obtained. Results analogous to those shown here were obtained with other comparable values of the peak intensities and signal shapes, as well as outside phase matching.

In conclusion, we predict that highly efficient second-harmonic generation of subpicosecond pulses can be accomplished in walk-off-compensated NPP organic crystals with peak pump intensities in the megawatts per square centimeter range, in a wide wavelength band centered around the third telecommunication window. Available diffraction gratings with suitable groove spacing can produce the required tilted pulses. The results presented here are believed to expand greatly the potential applications of NPP to the implementation of parametric devices and cascading phenomena in general.[13]

This work was supported by the Generalitat de Catalunya. Important remarks by J. Zyss and W. E. Torruellas are gratefully acknowledged. J. Torres's e-mail address is jperez@tsc.upc.es.

References

1. J. Zyss, J. F. Nicoud, and M. Coquillay, J. Chem. Phys. **81,** 4160 (1984).
2. I. Ledoux, C. Lepers, A. Perigaud, J. Baden, and J. Zyss, Opt. Commun. **80,** 149 (1990).
3. G. P. Banfi, P. K. Datta, V. Degiorgio, G. Donelli, D. Fortusini, and J. N. Sherwood, Opt. Lett. **23,** 439 (1998).
4. Z. Wang, D. J. Hagan, E. W. VanStryland, J. Zyss, P. Vidakovik, and W. E. Torruellas, J. Opt. Soc. Am. B **14,** 76 (1997).
5. V. D. Volosov, S. G. Karpenko, N. E. Kornienko, and V. L. Strizhevskii, Sov. J. Quantum Electron. **4,** 1090 (1975).
6. O. E. Martnez, IEEE J. Quantum Electron. **25,** 2464 (1989).
7. G. Szab and Z. Bor, Appl. Phys. B **50,** 51 (1990).
8. R. Danielius, A. Paskarskas, P. Di Trapani, A. Andreoni, C. Solcia, and P. Foggi, Opt. Lett. **21,** 973 (1996); A. Dubietis, G. Valiulis, G. Tamošauskas, D. Danielius, and A. Piskarskas, Opt. Lett. **22,** 1071 (1997); G. Valiulis, A. Dubietis, R. Danielius, D. Caironi, A. Visconti, and P. Di Trapani, J. Opt. Soc. Am. B **16,** 722 (1999).
9. P. Di Trapani, D. Caironi, G. Valiulis, R. Danielius, and A. Piskarskas, Phys. Rev. Lett. **81,** 570 (1998).
10. X. Liu, L. J. Qian, and F. W. Wise, Phys. Rev. Lett. **82,** 4631 (1999).
11. C. R. Menyuk, R. Schiek, and L. Torner, J. Opt. Soc. Am. B **11,** 2434 (1994).
12. P. K. Datta, D. Fortusini, G. Donelli, G. P. Banfi, V. Degiorgio, J. N. Sherwood, and G. C. Bhar, Opt. Commun. **149,** 331 (1998).
13. G. I. Stegeman, D. J. Hagan, and L. Torner, Opt. Quantum Electron. **28,** 1691 (1996).